INTERNATIONAL JOURNAL FOR NUMERICAL METHODS IN FLUIDS, VOL. 6, 427–443 (1986)

A FINITE ELEMENT APPROXIMATION OF THE UNSTEADY TWO-DIMENSIONAL NAVIER–STOKES EQUATIONS

F. N. VAN DE VOSSE

Department of Mechanical Engineering, Eindhoven University of Technology, PO BOX 513, 5600 MB Eindhoven, The Netherlands

A. SEGAL

Department of Mathematics and Informatics, Delft University of Technology, The Netherlands

A. A. VAN STEENHOVEN AND J. D. JANSSEN

Department of Mechanical Engineering, Eindhoven University of Technology, The Netherlands

SUMMARY

In this paper a penalty finite element solution method for the unsteady Navier–Stokes equations for two-dimensional incompressible flow is described. The performances of the Euler implicit (EI) and the Crank–Nicolson (CN) time integration methods are analysed. Special attention is payed to the undamped pressure oscillations which can occur when the Crank–Nicolson integration rule is used in combination with the penalty function method. Stability and convergence properties are illustrated by means of the computation of fully developed oscillating flow between two flat plates. Furthermore, the von Karman vortex street past a circular cylinder is computed to demonstrate the behaviour of the time integration schemes for a more complicated flow. It is concluded that the EI method has its advantages over the CN method with respect to the damping of numerical oscillations. However, for flows with an important convective contribution, where physically originated oscillations may be present, the CN method is preferable.

KEY WORDS Navier–Stokes Equations Time Integration Penalty Function Approach Oscillating Flow Vortex Shedding

INTRODUCTION

A 7-noded (P_2^+, P_1) triangular element (see Figure 1) for the Navier–Stokes equations satisfying the Brezzi–Babuska conditions is introduced by Crouzeix and Raviart.[1] As indicated by Griffiths[2] the number of degrees of freedom per element can be reduced from 17 to 13, by eliminating the velocity and pressure derivative parameters at the centroid of the element. The resulting modified element, together with a penalty function approach to the continuity equation has proved to be powerful for the steady Navier–Stokes equations.[3] In this study the applicability of this element for the unsteady Navier–Stokes equations is treated. The performances of the Euler implicit (EI) and the Crank–Nicolson (CN) integration schemes are analysed and compared. Sani *et al.*[4] mentioned undamped pressure oscillations when the CN-scheme is used in combination with the penalty function method. In this paper these oscillations will be related

0271–2091/86/070427–17$08.50

Received 1 January 1986
Revised 16 January 1986

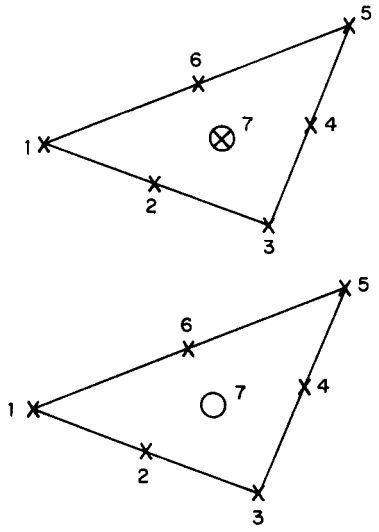

Figure 1. The extended quadratic triangular (P_2^+, P_1) element and its modification ($\times$: velocity, $\bigcirc$: pressure)

to general properties of the CN algorithm. Experiences with stability and convergence properties of the EI- and CN-integration will be illustrated by means of the computations of the fully developed oscillating flow between two parallel plates. Finally, computations of the von Karman vortex shedding past a circular cylinder are compared with data from numerical analysis[5] as well as experiments.[6]

GOVERNING EQUATIONS

The two-dimensional Navier–Stokes equations for incompressible Newtonian fluids are given by the momentum equations together with the continuity equation. In Cartesian co-ordinates these equations read (see, for instance, Reference 7):

$$\rho\frac{\partial u_i}{\partial t}+\sum_{j=1}^{2}\rho u_j\frac{\partial u_i}{\partial x_j}=\rho f_i+\sum_{j=1}^{2}\frac{\partial \sigma_{ij}}{\partial x_j}, \qquad i=1,2, \tag{1a}$$

$$\sum_{j=1}^{2}\frac{\partial u_j}{\partial x_j}=0. \tag{1b}$$

Here ρ denotes the density, u_i the ith component of the velocity and σ_{ij} the components of the Cauchy stress tensor:

$$\sigma_{ij}=-p\delta_{ij}+\eta\left(\frac{\partial u_i}{\partial x_j}+\frac{\partial u_j}{\partial x_i}\right), \qquad i,j=1,2, \tag{1c}$$

with p the pressure, δ_{ij} the Kronecker delta and η the dynamic viscosity. The boundary of the considered region Ω is denoted by Γ. The corresponding boundary conditions which specify the physical problem may be a combination of prescribed velocities and stresses in two independent directions:

$$u_j \quad \text{or} \quad \sigma_{ij}n_j \text{ prescribed on } \Gamma \quad \text{for} \quad j=1,2, \tag{2}$$

with $\mathbf{n}$ the outer normal on Γ. Furthermore, the initial velocity must be given.

SPATIAL DISCRETIZATION

In order to discretize (1) the standard Galerkin method is applied, starting from the weak formulation of (1). The velocity and pressure are approximated by a linear combination of time independent basis functions φ_{in} and ψ_m, respectively:

$$u_i^h = \sum_{n=1}^{N} u_{in}\varphi_{in}, \qquad i = 1,2, \tag{3a}$$

$$p^h = \sum_{m=1}^{M} p_m\psi_m. \tag{3b}$$

The basis functions φ_{in} $(i = 1,2; n = 1,\ldots,N)$ and ψ_m $(m = 1,\ldots,M)$ are used as test functions for (1a) and (1b), respectively. After use of (3), the following set of non-linear ordinary differential equations is obtained:

$$\mathbf{M}\dot{\mathbf{u}} + [\mathbf{S} + \mathbf{N}(\mathbf{u})]\mathbf{u} + \mathbf{L}^{\mathrm{T}}\mathbf{p} = \mathbf{f} + \mathbf{b}, \tag{4a}$$

$$\mathbf{L}\mathbf{u} = \mathbf{0}, \tag{4b}$$

with $\mathbf{u}$ a vector of length $2N$ containing the velocity parameters $u_{in}(i = 1,2;\ n = 1,\ldots,N)$ and $\mathbf{p}$ a vector of length M containing the pressure parameters $p_m(m = 1,\ldots,M)$. $\dot{\mathbf{u}}$ refers to differentiation of $\mathbf{u}$ with respect to time. Furthermore $\mathbf{M}$ is the mass matrix defined as $(k = 1,\ldots,N$ and $l = 1,\ldots,N)$

$$\mathbf{M} = \begin{bmatrix} \mathbf{M}^{11} & \mathbf{M}^{12} \\ \mathbf{M}^{21} & \mathbf{M}^{22} \end{bmatrix} \quad \text{with} \quad \mathbf{M}^{ij}(k,l) = \rho\delta_{ij}\int_{\Omega} \varphi_{ik}\varphi_{jl}\,\mathrm{d}\Omega, \tag{5a}$$

$\mathbf{S}$ is the diffusion matrix $(k = 1,\ldots,N$ and $l = 1,\ldots,N)$:

$$\mathbf{S} = \begin{bmatrix} \mathbf{S}^{11} & \mathbf{S}^{12} \\ \mathbf{S}^{21} & \mathbf{S}^{22} \end{bmatrix} \quad \text{with} \quad \mathbf{S}^{ij}(k,l) = \int_{\Omega} \eta\left[\sum_{\alpha=1}^{2}\left(\frac{\partial\varphi_{ik}}{\partial x_\alpha}\frac{\partial\varphi_{jl}}{\partial x_\alpha}\right)\delta_{ij} + \frac{\partial\varphi_{ik}}{\partial x_j}\frac{\partial\varphi_{jl}}{\partial x_i}\right]\mathrm{d}\Omega, \tag{5b}$$

$\mathbf{N}(\mathbf{u})\mathbf{u}$ is the non-linear convection term $(k = 1,\ldots,N)$:

$$[\mathbf{N}(\mathbf{u})\mathbf{u}]_k = \sum_{j=1}^{2}\int_{\Omega}\rho\left[\sum_{n=1}^{N} u_{jn}\varphi_{jn}\sum_{l=1}^{N} u_{il}\frac{\partial\varphi_{il}}{\partial x_j}\right]\varphi_{ik}\,\mathrm{d}\Omega, \tag{5c}$$

$\mathbf{L}$ is the divergence matrix $(m = 1,\ldots,N$ and $l = 1,\ldots,N)$:

$$\mathbf{L} = [\mathbf{L}^1 \quad \mathbf{L}^2] \quad \text{with} \quad \mathbf{L}^i(m,l) = -\int_{\Omega}\psi_m\frac{\partial\varphi_{il}}{\partial x_i}\,\mathrm{d}\Omega, \tag{5d}$$

$\mathbf{f}$ is the force vector $(k = 1,\ldots,N)$:

$$\mathbf{f} = [\mathbf{f}^1\,\mathbf{f}^2]^{\mathrm{T}} \quad \text{with} \quad \mathbf{f}^i(k) = \int_{\Omega}\rho f_i\varphi_{ik}\,\mathrm{d}\Omega \tag{5e}$$

and $\mathbf{b}$ is the boundary stress vector resulting from integration by parts of the diffusive and pressure terms in the momentum equations $(k = 1,\ldots,N)$:

$$\mathbf{b} = [\mathbf{b}^1\,\mathbf{b}^2]^{\mathrm{T}} \quad \text{with} \quad \mathbf{b}^i(k) = \int_{\Gamma}\sum_{j=1}^{2}\sigma_{ij}n_j\varphi_{ik}\,\mathrm{d}\Omega. \tag{5f}$$

THE EXTENDED QUADRATIC CONFORMING (P_2^+, P_1) ELEMENT

It is a well-known fact that finite elements for incompressible flows must satisfy the Brezzi–Babuska condition. This condition is necessary for the consistency of the equations.[8] When applying the penalty function method, the violation of the B–B condition can result in spurious (chequerboard) pressure modes.[9] An example of an element satisfying the B–B condition is the extended quadratic conforming (P_2^+, P_1) triangular element described by Crouzeix and Raviart.[1] The velocity is approximated by a quadratic function plus some third degree terms vanishing on the boundary of the element. The pressure is approximated linearly by the pressure and its derivatives in the centroid and hereby discontinuous over the element boundaries (see Figure 1). Per element the velocity and pressure approximations then read

$$u_i^h = \sum_{n=1}^{7} u_{in}\varphi_{in}, \tag{6a}$$

$$p^h = p_7\psi_1 + \left.\frac{\partial p}{\partial x_1}\right|_{\mathbf{x}_7} \psi_2 + \left.\frac{\partial p}{\partial x_2}\right|_{\mathbf{x}_7} \psi_3, \tag{6b}$$

with

$$\varphi_{in} = \begin{cases} \lambda_n(2\lambda_n - 1) + \lambda_1\lambda_2\lambda_3, & 1 \leqslant n \leqslant 3, \\ 4\lambda_1\lambda_2\lambda_3(1/\lambda_{n-3} - 3), & 4 \leqslant n \leqslant 6, \\ \lambda_1\lambda_2\lambda_3, & n = 7, \end{cases}$$

$$\psi_1 = 1,$$

$$\psi_2 = x - x_7,$$

$$\psi_3 = y - y_7.$$

Here λ_n are the barycentric co-ordinates of the element (see for instance Reference 8). This approximation leads to an error estimate of $O(h^3)$ for the velocity and of $O(h^2)$ for the pressure.[1] As indicated by Griffiths,[2] this element with 17 unknowns for the pressure (14 velocity and 3 pressure parameters) can be modified by eliminating the velocities and pressure derivatives in the centroid (see Appendix). The number of unknowns per element is then reduced from 17 to 13 (see Figure 1).

TIME INTEGRATION OF THE EQUATIONS

The time derivative in the discrete Navier–Stokes equations (4) is approximated by a finite difference θ-method. Considering the equation

$$\dot{\mathbf{u}} = \mathbf{f}, \tag{7}$$

this approximation is defined by

$$\frac{\mathbf{u}^{n+1} - \mathbf{u}^n}{\Delta t} = \mathbf{f}^{n+\theta}, \tag{8}$$

with

$$\mathbf{f}^{n+\theta} = \theta\mathbf{f}^{n+1} + (1-\theta)\mathbf{f}^n, \qquad 0 \leqslant \theta \leqslant 1.$$

For $\theta = 0$ and $\theta = 1$ this scheme reduces to the Euler explicit (EE) and Euler implicit (EI) methods, respectively, both $O(\Delta t)$ accurate for linear equations. For $\theta = 0{\cdot}5$ the scheme becomes the Crank–Nicolson scheme (CN) which is of $O(\Delta t^2)$ for linear equations.

In order to make a proper choice for the value of θ, the time integration of a linear set of ordinary differential equations resulting from the discretization of a parabolic differential equation is considered:

$$\dot{\mathbf{u}} = \mathbf{A}\mathbf{u} + \mathbf{f}, \tag{9a}$$

$$\mathbf{u}(t_0) = \mathbf{u}_0. \tag{9b}$$

Here $\mathbf{A}$ is assumed to be an $N \times N$ matrix with real coefficients resulting from a linear elliptic differential operator. Furthermore it is assumed that $\mathbf{A}$ is non-defect, i.e. has N linear independent eigenvectors (If $\mathbf{A}$ is defect a more complicated analysis yields almost the same conclusions). Owing to the linear independence to the N eigenvectors, a non-singular matrix $\mathbf{B}$ with complex coefficients exists, defined by

$$\mathbf{AB} = \mathbf{B}\Lambda, \tag{10a}$$

with $\Lambda = \text{diag}(\lambda_1, \ldots, \lambda_N)$ and $\lambda_1, \ldots, \lambda_N$ the eigenvalues of $\mathbf{A}$. The differential equation and also its discretized approximation is called stable when a finite error $\boldsymbol{\varepsilon}_0$ in the initial condition $\mathbf{u}_0$ results in a finite error $\boldsymbol{\varepsilon}(t)$ in $\mathbf{u}(t)$, for any t. To evaluate this error propagation two cases are considered:

(1) $\mathbf{u}$ is a solution of (9a) with $\mathbf{u}(t_0) = \mathbf{u}_0$

(2) $\boldsymbol{\xi}$ is a solution of (9a) with $\boldsymbol{\xi}(t_0) = \mathbf{u}_0 + \boldsymbol{\varepsilon}_0$
with $\boldsymbol{\varepsilon}_0$ a small perturbation of $\mathbf{u}_0$.

If $\boldsymbol{\varepsilon}$ is defined as $\boldsymbol{\varepsilon} = \boldsymbol{\xi} - \mathbf{u}$ then $\dot{\boldsymbol{\varepsilon}} = \mathbf{A}\boldsymbol{\varepsilon}$ and $\boldsymbol{\varepsilon}(t_0) = \boldsymbol{\varepsilon}_0$ or, since $\mathbf{B}$ is non-singular, $\boldsymbol{\eta} = \mathbf{B}^{-1}\boldsymbol{\varepsilon}$ can be defined and thus

$$\dot{\boldsymbol{\eta}} = \Lambda\boldsymbol{\eta}, \tag{10b}$$

with

$$\boldsymbol{\eta}(t_0) = \mathbf{B}^{-1}\boldsymbol{\varepsilon}_0 \equiv \boldsymbol{\eta}_0.$$

The solution of (10b) then can be written as

$$\eta_i = \eta_{i0} e^{\lambda_i (t - t_0)}, \qquad i = 1, \ldots, N. \tag{11}$$

In order that the differential equation is stable, η_i must be a non-increasing function of time; hence

$$\text{Re}[\lambda_i] \leqslant 0 \tag{12}$$

must hold for any $i (i = 1, \ldots, N)$.

Numerical time integration schemes generally lead to equations for $\boldsymbol{\eta}$ of the form

$$\boldsymbol{\eta}^{n+1} = \mathbf{G}\boldsymbol{\eta}^n, \tag{13}$$

with $\mathbf{G}$ the so-called multiplication matrix and $\boldsymbol{\eta}^n = \boldsymbol{\eta}(t_n)$. For stability of the numerical scheme it is necessary that $\|\mathbf{G}\| \leqslant 1$ (with $\|\mathbf{G}\|$ any regular vector norm). For the θ-method one easily verifies that this leads to

$$|c_i| = \left| \frac{1 + (1 - \theta)\lambda_i \Delta t}{1 - \theta \lambda_i \Delta t} \right| < 1, \qquad i = 1, \ldots, N. \tag{14}$$

In Figure 2 the stability regions of $\lambda_i \Delta t$ are given for the interval $0 \leqslant \theta \leqslant 1$. For $0{\cdot}5 \leqslant \theta \leqslant 1$ the scheme appears to be stable for all $\lambda \Delta t$. For $0 \leqslant \theta < 0{\cdot}5$ the scheme is only conditionally stable. In the case that the eigenvalues of $\mathbf{A}$ are large (but negative), relatively small time steps Δt have to be applied to ensure stability.

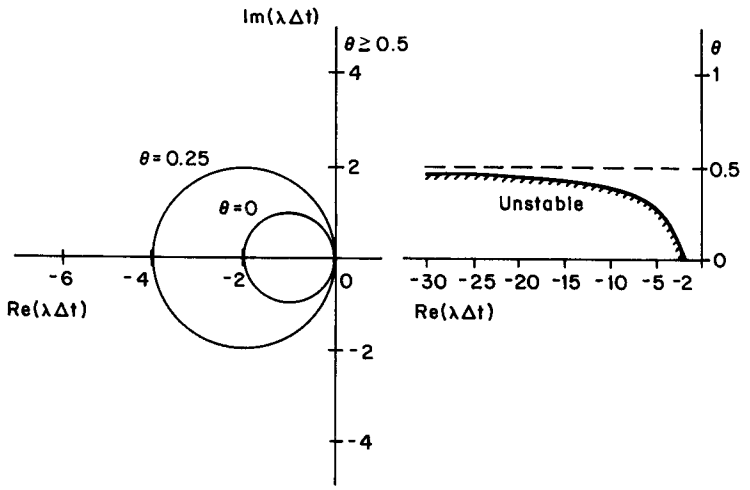

Figure 2. Stability regions of the θ-method for complex and real eigenvalues, respectively

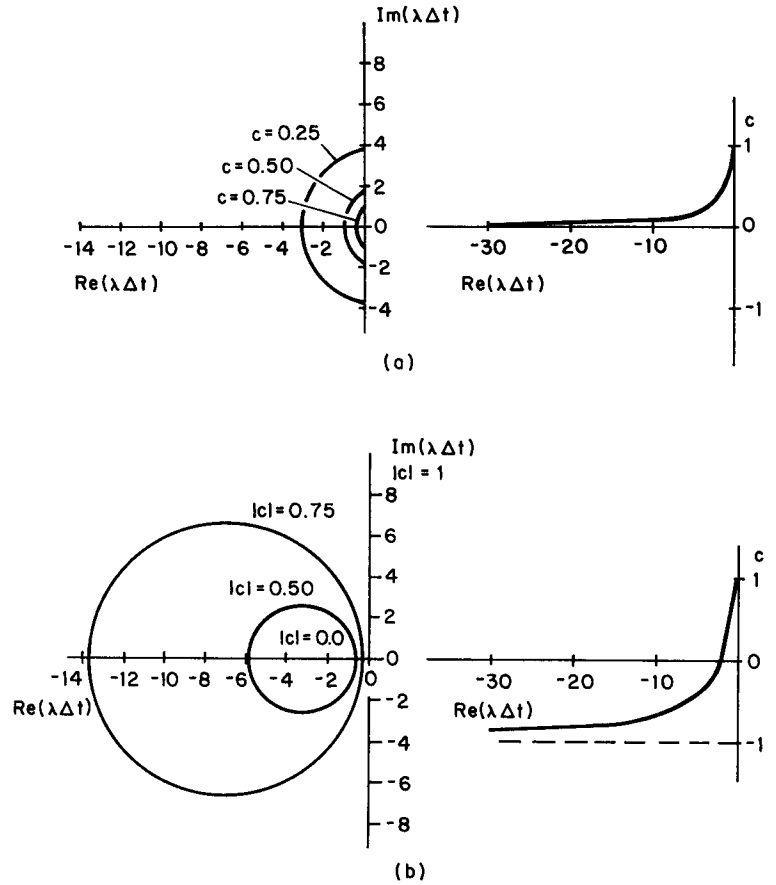

Figure 3. Amplification factor c as a function of $(\lambda\Delta t)$ for the EI (a) and the CN (b) methods for complex and real eigenvalues, respectively

In Figures 3(a) and 3(b), the amplification factor c_i is plotted as function of $\mathrm{Re}[\lambda\Delta t]$ for $\theta = 1$ and $\theta = 0{\cdot}5$, respectively. From these Figures it can be observed that for $\theta = 0{\cdot}5$ (CN) the amplification tends to -1 for large negative eigenvalues, whereas for $\theta = 1$ (EI) the amplification tends to 0. To indicate whether one θ-value is preferable to another, the eigenvalues of the system to be solved have to be known. In the case of large negative and real eigenvalues, computational errors or errors in the initial condition damp very slowly for the CN-scheme and will produce an oscillatory behaviour because the amplification factor tends to -1. On the contrary, these errors will be damped very fast by the EI-method. However, in the case when **A** is a non-symmetric matrix, the eigenvalues will also have an imaginary part, and will drift into the complex plane. The situation with complex eigenvalues is more complicated, since for a dominating imaginary part of the eigenvalues, oscillations are inherent to the solution. From Figure 3 it is seen that if Δt is too large, the EI method will also damp these oscillations. However, for complex eigenvalues with a dominating real part, the behaviour of the time integration is similar to the behaviour in the situation with real eigenvalues.

PENALTY FUNCTION APPROACH

Application of the θ-method of time integration on (4) gives

$$\{\mathbf{M} + \theta\Delta t[\mathbf{S} + \mathbf{N}(\mathbf{u}^{n+1})]\}\mathbf{u}^{n+1} + \theta\Delta t\mathbf{L}^{\mathrm{T}}\mathbf{p}^{n+1} = \Delta t(\mathbf{f}^{n+\theta} + \mathbf{b}^{n+\theta}) + \{\mathbf{M} - (1-\theta)\Delta t[\mathbf{S} + \mathbf{N}(\mathbf{u}^n)]\}\mathbf{u}^n - (1-\theta)\Delta t\mathbf{L}^{\mathrm{T}}\mathbf{p}^n, \tag{15a}$$

$$\mathbf{L}\mathbf{u}^{n+1} = \mathbf{0}. \tag{15b}$$

The direct solution of the set of equations (15) is time and memory consuming. This is caused by the fact that zero components appear on the principal diagonal of the coefficient matrix, owing to the absence of the pressure in the continuity equation. Therefore a partial pivoting procedure is necessary, which disturbs the band structure of the matrix. To overcome this difficulty, the penalty function method is applied. To that end the continuity equation is perturbed and replaced by

$$\sum_{j=1}^{2} \frac{\partial u_j}{\partial x_j} = -\varepsilon p, \tag{16}$$

where ε is a small parameter. Reddy[10] showed that for the steady Stokes equations the error due to this perturbation is of $O(\varepsilon)$, whereas for the Navier–Stokes equations the error is at most of $O(\varepsilon^{1/2})$. However, his numerical experiments showed a convergence behaviour of order ε in both cases. The main advantage of the penalty method over the direct solution of (15) is that the pressure is eliminated from the momentum equations, resulting in a smaller set of equations that can be solved without pivoting procedures. The pressure can then be obtained, after solving the perturbed momentum equations, by simple matrix–vector multiplication, i.e.

$$\{\mathbf{M} + \theta\Delta t[\mathbf{S} + \mathbf{N}(\mathbf{u}^{n+1}) + \frac{1}{\varepsilon}\mathbf{L}^{\mathrm{T}}\mathbf{M}_{\mathrm{p}}\mathbf{L}]\}\mathbf{u}^{n+1} = \Delta t(\mathbf{f}^{n+\theta} + \mathbf{b}^{n+\theta}) + \{\mathbf{M} - (1-\theta)\Delta t[\mathbf{S} + \mathbf{N}(\mathbf{u}^n) + \frac{1}{\varepsilon}\mathbf{L}^{\mathrm{T}}\mathbf{M}_{\mathrm{p}}\mathbf{L}]\}\mathbf{u}^n, \tag{17a}$$

$$\mathbf{p}^{n+1} = \frac{1}{\varepsilon}\mathbf{M}_{\mathrm{p}}\mathbf{L}\mathbf{u}^{n+1}, \tag{17b}$$

with

$$\mathbf{M}_p(k,l) = \int_\Omega \psi_k \psi_l \, d\Omega, \qquad k,l = 1,\ldots,M. \tag{17c}$$

This set of non-linear equations is solved by one step of a Newton–Raphson method, leading to

$$\left\{\mathbf{M} + \theta\Delta t\left[\mathbf{S} + \mathbf{J}(\mathbf{u}^n) + \frac{1}{\varepsilon}\mathbf{L}^T\mathbf{M}_p\mathbf{L}\right]\right\}\mathbf{u}^{n+1}$$
$$= \Delta t(\mathbf{f}^{n+\theta} + \mathbf{b}^{n+\theta}) + \left\{\mathbf{M} - (1-\theta)\Delta t\left[\mathbf{S} + \frac{1}{\varepsilon}\mathbf{L}^T\mathbf{M}_p\mathbf{L}\right]\right\}\mathbf{u}^n$$
$$- (1-2\theta)\Delta t\mathbf{N}(\mathbf{u}^n)\mathbf{u}^n, \tag{18a}$$

$$\mathbf{p}^{n+1} = \frac{1}{\varepsilon}\mathbf{M}_p\mathbf{L}\mathbf{u}^{n+1}, \tag{18b}$$

with $\mathbf{J}(\mathbf{u}^n)$ the Jacobian matrix of $\mathbf{N}(\mathbf{u}^n)$. For stationary equations the following Newton–Raphson iteration can be used:

$$\left[\mathbf{S} + \mathbf{J}(\mathbf{u}^\nu) + \frac{1}{\varepsilon}\mathbf{L}^T\mathbf{M}_p\mathbf{L}\right]\mathbf{u}^{\nu+1} = \mathbf{f} + \mathbf{b} + \mathbf{N}(\mathbf{u}^\nu)\mathbf{u}^\nu, \qquad \nu = 0,\ldots,\nu_m, \tag{19a}$$

$$\mathbf{p}^{\nu_m+1} = \frac{1}{\varepsilon}\mathbf{M}_p\mathbf{L}\mathbf{u}^{\nu_m+1}. \tag{19b}$$

The iteration can be stopped when $\|\mathbf{u}^{\nu+1} - \mathbf{u}^\nu\| < \delta$, δ being the required accuracy.

STABILITY AND ACCURACY OF THE TIME INTEGRATION

The stability and accuracy of the time integration methods described are elucidated by computations of oscillating flow in a channel (two parallel plates) and the vortex shedding past a cylinder. The oscillating channel flow is chosen because an exact solution can be derived. Moreover, this flow problem is of physiological interest to the analysis of blood flow in arteries (the premise of our research). The non-linear convective terms are neglected, and only real eigenvalues occur. To obtain an idea of the influence of an imaginary part of the eigenvalues on the behaviour of the time integration, the vortex shedding phenomenon is also analysed. Then the convective terms do play an important role.

Fully developed oscillating flow between two parallel plates

To elucidate the stability and accuracy of the time integrations used, the development from rest of oscillating flow between two parallel plates was analysed. For convenience an oscillating parabolic velocity profile was used as the in-stream condition (see Figure 4).

Another way to analyse the fully developed oscillating channel flow is to use an oscillatory normal stress at the in-stream instead of the Dirichlet conditions used here. Then only one element in the x-direction is needed since the pressure only varies linearly and the velocity does not change at all in that direction. However, this has two important disadvantages compared with the Dirichlet boundary conditions. First, the pressure is then found to be independent of the time step used. In fact the pressure is prescribed indirectly by the normal stresses. Secondly,

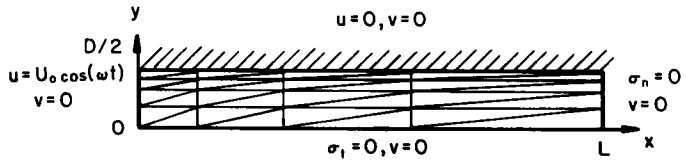

Figure 4. Geometry and boundary conditions for the oscillating channel flow problem ($L = 15D$), U_0 = parabolic profile

a rather long transition of about 20 time cycles was found before the velocity was fully developed in time. The errors for the velocity were observed to be of the same order as in the problem with the Dirichlet boundary conditions.

The exact solution of the fully developed flow can be determined in an analogous way to the fully developed oscillating flow in a circular cylinder[11] and is given by

$$u = \mathrm{Re}\left[Q_0 \left\{ \frac{1 - K(\alpha, y/D)}{1 - P(\alpha)} \right\} e^{i\omega t} \right], \qquad v = 0, \tag{20a}$$

$$\frac{\partial p}{\partial x} = \mathrm{Re}\left[-i\omega Q_0 \left\{ \frac{1}{1 - P(\alpha)} \right\} e^{i\omega t} \right], \qquad \frac{\partial p}{\partial y} = 0, \tag{20b}$$

with Q_0 the flow amplitude ($Q_0 = \frac{2}{3} U_0 D$), D the channel height, U_0 the velocity amplitude, and

$$K(\alpha, y) = \frac{e^{\alpha\sqrt{(iy/D)}} + e^{-\alpha\sqrt{(iy/D)}}}{e^{\alpha\sqrt{i}} + e^{-\alpha\sqrt{i}}}, \tag{21a}$$

$$P(\alpha) = \frac{1}{\alpha\sqrt{i}} \frac{e^{\alpha\sqrt{i}} - e^{-\alpha\sqrt{i}}}{e^{\alpha\sqrt{i}} + e^{-\alpha\sqrt{i}}}, \tag{21b}$$

$$\alpha = D\sqrt{(\omega/\nu)}. \tag{21c}$$

Re[..] is the real part of [..] and $i = \sqrt{(-1)}$.

The solution is approximated by solving the unsteady Stokes equations for an angular frequency $\omega = 2\pi$ [s^{-1}], a viscosity $\nu = 3{\cdot}5 \times 10^{-6}$ [$m^2 s^{-1}$] and a channel height $D = 0{\cdot}6 \times 10^{-2}$[m]. This leads to a physiological value of the frequency parameter $\alpha \approx 8$. The length of the channel was taken to be $15D$. As the pressure derivative did not change in the first 3 significant decimals in the last and last but one element upstream of the outlet, the conclusion is justified that the assumed channel length is sufficient to guarantee a fully developed oscillating flow at the outlet. Comparison of numerical and analytical solutions is done for different θ-values in the time integration with time steps of 0·2, 0·1 and 0·05 times the cycle period of the flow ($\Delta t = 0{\cdot}2$, $\Delta t = 0{\cdot}1$, $\Delta t = 0{\cdot}05$ s), respectively, and with the aid of the following error definitions

$$\Delta u = \left. \frac{\left[\int_0^{D/2} (u - u^h)^2 \, dy \right]^{1/2}}{\left[\int_0^{D/2} u^2 \, dy \right]^{1/2}} \right|_{x = 15D,} \tag{22a}$$

$$\Delta p_x = \left. \frac{\left| \frac{\partial p}{\partial x} - \frac{\partial p^h}{\partial x} \right|}{\left| \frac{\partial p}{\partial x} \right|} \right|_{x = 15D, \quad y = 0.} \tag{22b}$$

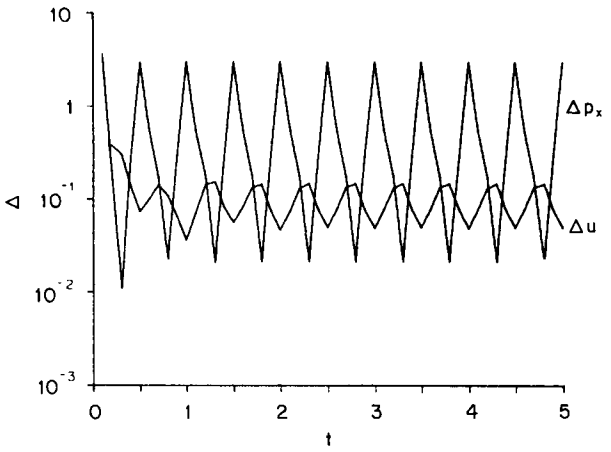

Figure 5(a). Relative errors in the velocity and pressure gradients at the out stream for the EI method plotted as a function of time for $\Delta t = 0{\cdot}1$

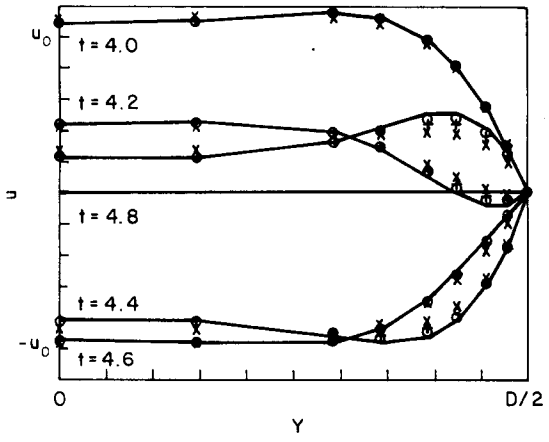

Figure 5(b). Velocity profiles at the out stream for $4{\cdot}0 \leqslant t \leqslant 4{\cdot}8$ (− : exact, × : $\Delta t = 0{\cdot}2$, + : $\Delta t = 0{\cdot}1$, ○ : $\Delta t = 0{\cdot}05$) for the EI method

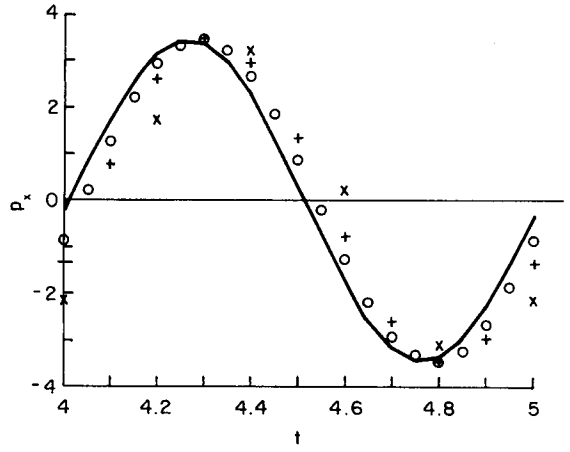

Figure 5(c). Pressure gradients at the out stream for $4{\cdot}0 \leqslant t \leqslant 5{\cdot}0$ (− : exact, × : $\Delta t = 0{\cdot}2$, + : $\Delta t = 0{\cdot}1$, ○ : $\Delta t = 0{\cdot}05$) for the EI method

Table I Time averaged relative errors in the velocity and the pressure gradient for the EI, CN and ISCN methods, respectively

Method	Euler implicit		Crank–Nicolson		CN with implicit start	
Δt	Δu	Δp_x	Δu	Δp_x	Δu	Δp_x
0·20	0·16	2·13	0·05	5·15	—	—
0·10	0·09	1·01	0·03	4·19	0·02	0·57
0·05	0·05	0·40	0·02	0·76	—	—

As expected from (14) the time integration was unstable for $0 \leqslant \theta < 0{\cdot}5$ for all time steps used. The large negative eigenvalues resulting from the penalty function method would require time steps of order ε. Because θ-values in the range $0{\cdot}5 < \theta < 1$ are not expected to give better accuracy then the first order EI-method ($\theta = 1$), only the EI and CN time integration were analysed in detail.

The Euler implicit scheme (EI). In Figure 5(a) the relative errors as defined in (22) are plotted against the time for the first five periods of the flow oscillation. The time step used was $\Delta t = 0{\cdot}1$. Figures 5(b) and 5(c) show the velocity profiles and pressure gradient approximations in the fifth period for $\Delta t = 0{\cdot}2$, $\Delta t = 0{\cdot}1$ and $\Delta t = 0{\cdot}05$, respectively, together with the exact solution. The corresponding errors were averaged in time and are given as functions of Δt in Table I. The large errors found for the pressure derivatives are attributed to the phase-lack between the exact and approximated solutions, as is visible in Figure 5(c).

The Crank–Nicolson scheme (CN). The same analysis was performed for the case that the CN-scheme was used (Figures 6(a)–(c) and Table I). From these results it is concluded that the CN-scheme gives considerably better velocity approximations, but worse pressure approximations. As can be seen from Figure 6(c), the poorer pressure approximations are the result of undamped oscillations. These oscillations are the consequence of the amplification factor tending to -1 for high negative eigenvalues of the coefficient matrix.

The Crank–Nicolson scheme with an implicit start (ISCN). Better results are obtained when the errors induced by the arbitrary initial value ($U_0 = 0$) are damped by an implicit start of the CN-scheme. In Figure 7 the results of the EI, the CN and the ISCN schemes are given (for averaged values see Table I). In the ISCN scheme the first period of the flow oscillation was integrated with the EI scheme. The results of the CN scheme are considerably improved when an implicit start is used to damp the errors induced by the assumed initial value.

Although the errors found for the velocity approximation are acceptable, relatively large errors are found for the pressure. These large errors are partly due to the large time steps that are used, and they are partly caused by the phase-lack between exact and numerical solutions. Smaller time steps were not applied, as then a finer grid had to be used to ensure that the time integration errors were much larger then the errors caused by the space discretization. However, no other conclusions are expected and therefore the present results are regarded as giving a good picture of the time integration methods applied.

Vortex shedding behind a circular cylinder

To evaluate the behaviour of the two time integration methods in a more complicated flow situation, the vortex shedding behind a circular cylinder with a diameter $D = 1$ was simulated.

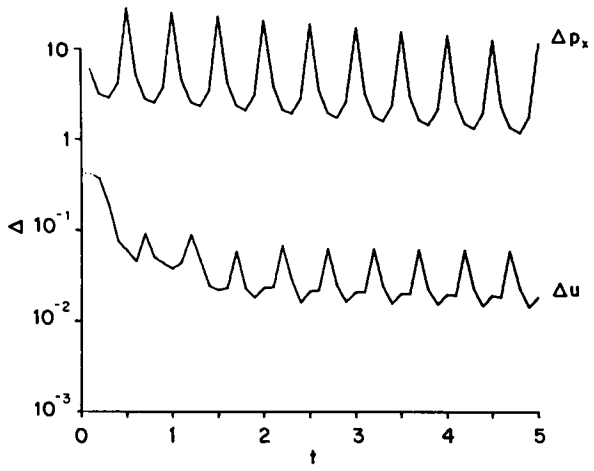

Figure 6(a). Relative errors in the velocity and pressure gradients at the out stream for the CN method plotted as a function of time for $\Delta t = 0{\cdot}1$

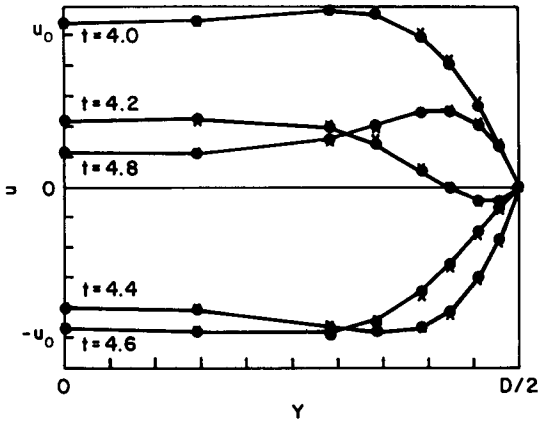

Figure 6(b). Velocity profiles at the out stream for $4{\cdot}0 \leqslant t \leqslant 4{\cdot}8$ (−: exact, ×: $\Delta t = 0{\cdot}2$, +: $\Delta t = 0{\cdot}1$, ○: $\Delta t = 0{\cdot}05$) for the CN method

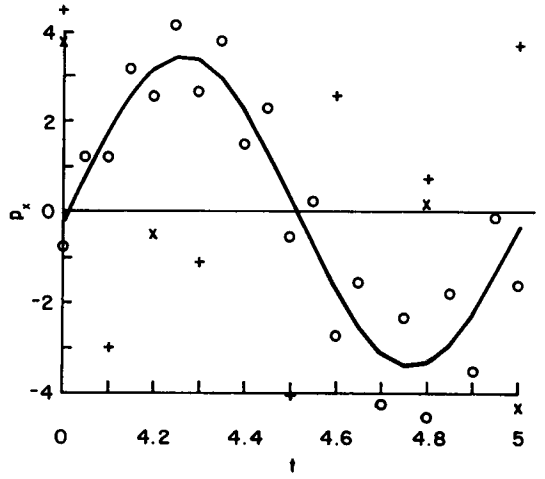

Figure 6(c). Pressure gradients at the out stream for $4{\cdot}0 \leqslant t \leqslant 5{\cdot}0$ (−: exact, ×: $\Delta t = 0{\cdot}2$, +: $\Delta t = 0{\cdot}1$, ○: $\Delta t = 0{\cdot}05$) for the CN method

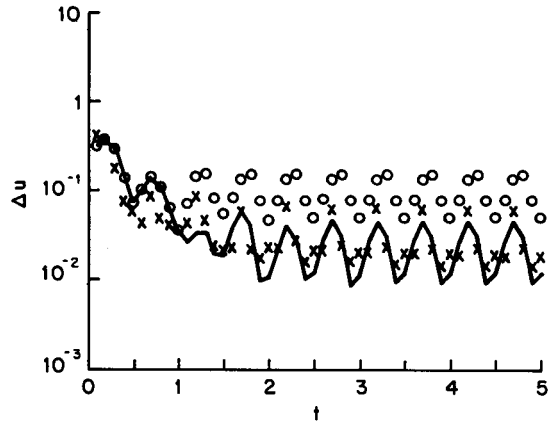

Figure 7(a). Relative errors in the velocity at the out stream for the EI(○), CN(×) and the ISCN(−), respectively, for $\Delta t = 0{\cdot}1$

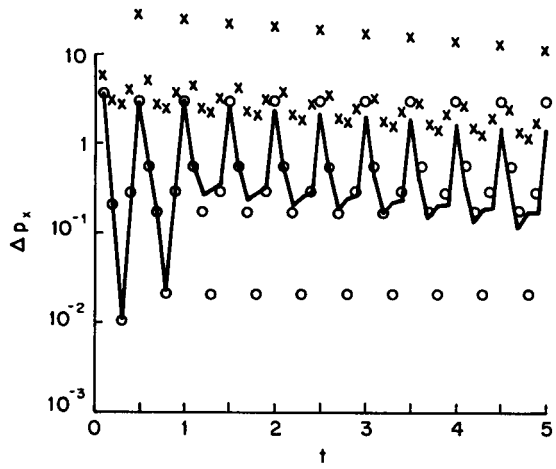

Figure 7(b). Relative errors in the pressure gradient at the out stream for the EI(○), CN(×) and the ISCN(−), respectively, for $\Delta t = 0{\cdot}1$

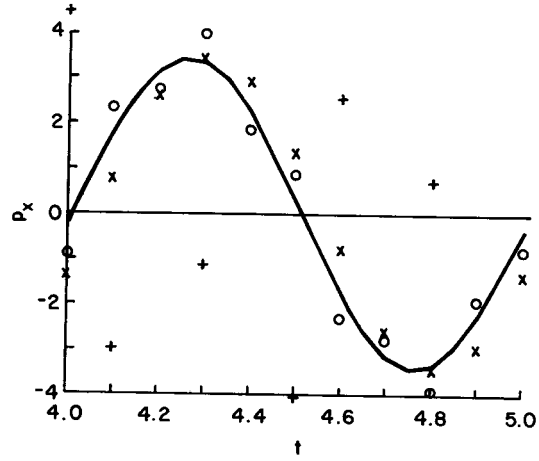

Figure 7(c). Pressure gradients in the last period at the out stream for the EI(×), CN(+), ISCN(○), respectively, for $\Delta t = 0.1$

The geometry was choosen equal to the geometry used by Gresho *et al.*[5] and is shown in Figure 8(a). Uniform Dirichlet inflow boundary conditions ($u = U_0 = 1, v = 0$) and stress-free outflow conditions were used, together with moving wall conditions ($u = 1, v = 0$) at the upper and lower walls. Both the Euler implicit and the Crank–Nicolson time integration methods arrived at a steady solution after about 30 time steps of $\Delta t = 1$. Owing to the symmetry of the mesh and boundary conditions, the vortex shedding was not generated spontaneously. To trigger the vortex shedding, the steady solution was disturbed in one time step by setting the velocity of the cylinder to 0·1 in the y-direction. Next, 10 EI time steps were performed to damp this distortion and to avoid hereby a too important influence on the flow field. After these implicit steps both integration schemes were applied with times steps $\Delta t = 1$, resulting in a periodic shedding cycle as shown in Figure 8(b), where the velocity component in the y-direction at $(x, y) = (10, 0)$ is plotted as a function of time. With the EI time integration the amplitude of the velocity component turns out to be an order smaller in magnitude than when the CN scheme was used. Furthermore, the amplitude damps rapidly for increasing time. In Figure 8(c) this velocity component is given for the CN method. The amplitude of these fluctuations agrees with the amplitude found by Gresho *et al.*[5] The Strouhal number (fD/U_0) of the vortex shedding is predicted to be 0·17. Experiments by Tritton[6] showed a Strouhal number of 0·16 for $Re = 100$. The performances of the EI scheme are expected to be better at smaller time steps. Anyhow, it can be concluded that, although the EI time integration has its advantages with respect to the numerical stability of the solution, this first-order scheme is far less applicable than the CN scheme in simulations of flows with an important convective property, such as the vortex shedding process.

CONCLUDING REMARKS

The behaviour of the Euler implicit and Crank–Nicolson time integration schemes for the unsteady Stokes equations using a penalty finite element method can be explained by a simple stability analysis of linear parabolic differential equations in general. In that case, the performances of the integration methods for eigenvalues of the system of equations with a large negative real part are important with respect to possible numerical oscillations of the solution. The first order EI algorithm has an amplification factor approaching zero when the real part of the eigenvalue goes to minus infinity. Therefore errors induced by the computation or errors due to the initial condition (often a steep velocity gradient in time) damp very quickly. Contrarily, the more accurate second order Crank–Nicolson rule gives rise to an amplification factor tending to -1, and therefore an oscillatory propagation of the introduced errors is expected. This phenomenon is illustrated by the analysis of the oscillating channel flow and is mainly visible in the poorer pressure approximations. If the disturbance of the initial value is damped out by a fully implicit time integration, the pressure oscillations observed, for the (smooth) boundary conditions used here, were reduced significantly. Finally it is assumed that the stability properties are thought to be affected mostly by the penalty parameter. The non-linear convective terms give rise to complex eigenvalues. These are not expected to lead to much different stability properties. However, the physically originated oscillatory properties of the solution of the differential equations can be damped incorrectly by the EI scheme. The CN method with an implicit start is preferable then. This statement is confirmed by the computation of the vortex shedding behind a circular cylinder.

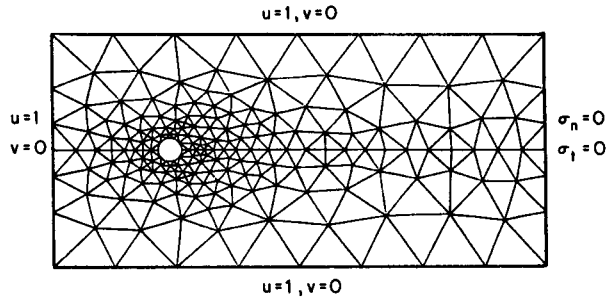

Figure 8(a). Geometry, mesh and boundary conditions for the vortex shedding computation

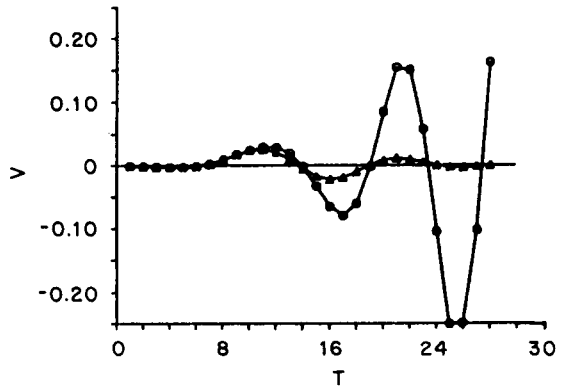

Figure 8(b). Velocity component in y-direction as a function of time: distortion at $t = 1s$, $0 < t \leqslant 10$ (EI, $\Delta t = 1$), $t > 10$ (▲: EI, $\Delta t = 1$, ○: CN, $\Delta t = 1$)

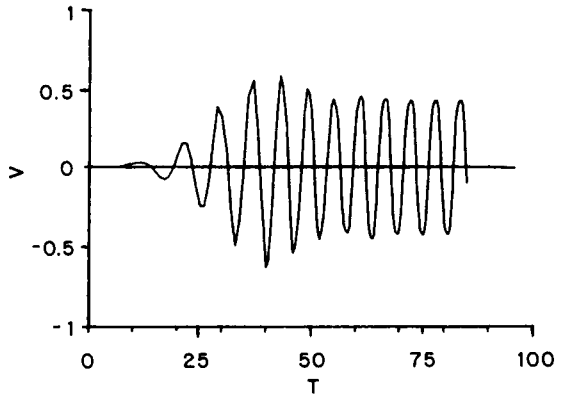

Figure 8(c). Velocity component in y-direction as a function of time: distortion at $t = 1$, $0 < t \leqslant 10$ (EI, $\Delta t = 1$), $10 < t \leqslant 40$ (CN, $\Delta t = 1$), $40 < t \leqslant 55$ (CN, $\Delta t = 0{\cdot}5$), $55 < t \leqslant 85$ (CN, $\Delta t = 0{\cdot}25$)

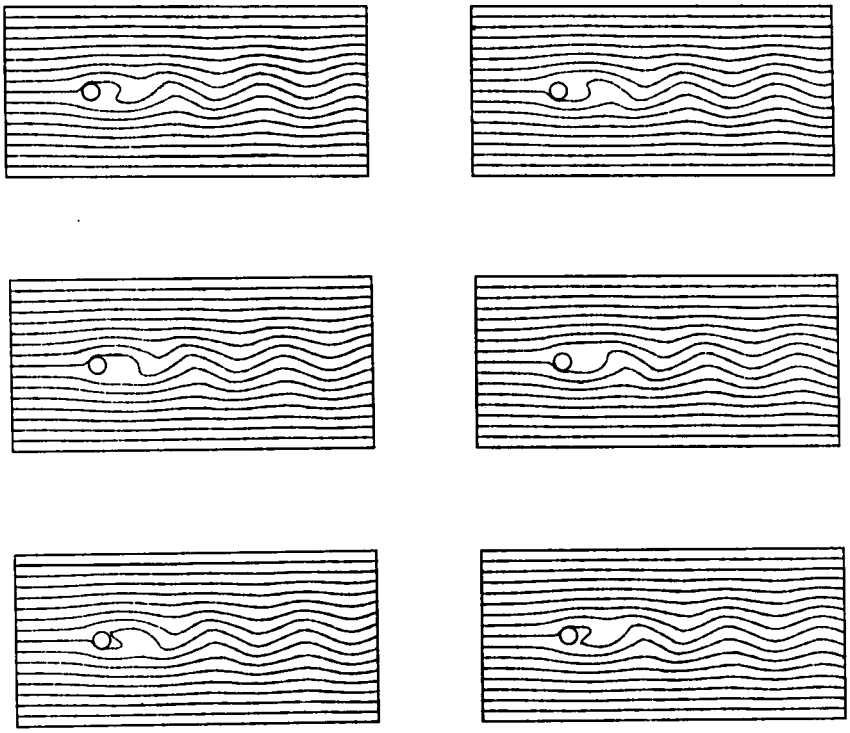

Figure 8(d). Streamline pattern during a shedding cycle (time difference 1 s)

APPENDIX

To eliminate the pressure gradients and velocities at the centroid, equations (4) are split into

$$\begin{bmatrix} \mathbf{M}_{11} & \mathbf{0} \\ \mathbf{0} & \mathbf{M}_{22} \end{bmatrix} \begin{bmatrix} \dot{\hat{\mathbf{u}}} \\ \dot{\mathbf{u}}_c \end{bmatrix} + \begin{bmatrix} \mathbf{K}_{11} & \mathbf{K}_{12} \\ \mathbf{K}_{21} & \mathbf{K}_{22} \end{bmatrix} \begin{bmatrix} \hat{\mathbf{u}} \\ \mathbf{u}_c \end{bmatrix} + \begin{bmatrix} \mathbf{L}_{11}^T & \mathbf{L}_{21}^T \\ \mathbf{L}_{12}^T & \mathbf{L}_{22}^T \end{bmatrix} \begin{bmatrix} \mathbf{p}_c \\ \mathbf{p}_\nabla \end{bmatrix} = \begin{bmatrix} \hat{\mathbf{f}} + \hat{\mathbf{b}} \\ \mathbf{f}_c + \mathbf{b}_c \end{bmatrix}, \tag{23a}$$

$$\begin{bmatrix} \mathbf{L}_{11} & \mathbf{L}_{12} \\ \mathbf{L}_{21} & \mathbf{L}_{22} \end{bmatrix} \begin{bmatrix} \hat{\mathbf{u}} \\ \mathbf{u}_c \end{bmatrix} = \begin{bmatrix} \mathbf{0} \\ \mathbf{0} \end{bmatrix}, \tag{23b}$$

with $\mathbf{K} = \mathbf{S} + \mathbf{N}(\mathbf{u})$. The velocity $\mathbf{u}$ is split into a part $\hat{\mathbf{u}}$ containing the velocities at the vertices and the midpoints of the sides of the elements, and a part $\mathbf{u}_c$ containing the velocities at the centroid. The pressure parameters are split into a part $\mathbf{p}_c$ containing the pressure at the centroids of the elements and a part $\mathbf{p}_\nabla$, containing the pressure derivatives at the centroids. The elimination of the centroid velocities can be performed with the aid of the second part of the continuity equation:

$$\mathbf{u}_c = -\mathbf{L}_{22}^{-1}\mathbf{L}_{21}\hat{\mathbf{u}} \equiv \mathbf{R}_0\hat{\mathbf{u}}, \tag{24}$$

with $\mathbf{R}_0$ a $2M \times (2N - 2M)$ square matrix. The inverse of $\mathbf{L}_{22}$ can easily be obtained element by element because of the discontinuity of the basis functions ψ_k. Since φ_{i7} vanishes on the element boundary the element matrix $\mathbf{L}_{22}^e$ reads

$$\mathbf{L}_{22}^e(i,k) = -\int_{\Omega^e} \psi_{k+1} \frac{\partial \varphi_{i7}}{\partial x_i} \mathrm{d}\Omega^e = \delta_{ki} \int_{\Omega^e} \varphi_{i7}\, \mathrm{d}\Omega^e, \qquad i,k = 1,2. \tag{25}$$

Furthermore it can be proved that $\mathbf{L}_{12} = \mathbf{0}$, since

$$\mathbf{L}_{12}^{e}(i,1) = -\int_{\Omega^e} \psi_1 \frac{\partial \varphi_{i7}}{\partial x_i} \mathrm{d}\Omega^e = \int_{\Omega_e} \frac{\partial \psi_1}{\partial x_i} \varphi_{i7} \, \mathrm{d}\Omega^e - \int_{\Gamma^e} \psi_1 \varphi_{i7} \, \mathrm{d}\Gamma^e, \qquad i = 1,2 \tag{26}$$
$$= \mathbf{0}.$$

Pre-multiplication on (23a) by $[\mathbf{I}_0^{\mathrm{T}} \ \mathbf{R}_0^{\mathrm{T}}]$ with $\mathbf{I}_0$ a $(2N-2M) \times (2N-2M)$ unity matrix, and substitution of (24) leads to

$$\hat{\mathbf{M}}\hat{\mathbf{u}} + \hat{\mathbf{K}}\hat{\mathbf{u}} + \hat{\mathbf{L}}^{\mathrm{T}}\mathbf{p}_c = \hat{\mathbf{f}} + \hat{\mathbf{b}},$$
$$\hat{\mathbf{L}}\hat{\mathbf{u}} = \mathbf{0}, \tag{27}$$

with

$$\hat{\mathbf{A}} = \mathbf{A}_{11} + \mathbf{R}_0^{\mathrm{T}}\mathbf{A}_{21} + \mathbf{A}_{12}\mathbf{R}_0 + \mathbf{R}_0^{\mathrm{T}}\mathbf{A}_{22}\mathbf{R}_0, \qquad \mathbf{A} = \mathbf{M}, \mathbf{K},$$
$$\hat{\mathbf{L}} = \mathbf{L}_{11},$$
$$\hat{\mathbf{c}} = [\mathbf{I}_0^{\mathrm{T}} \ \mathbf{R}_0^{\mathrm{T}}]\mathbf{c}, \qquad \mathbf{c} = \mathbf{f}, \mathbf{b}, \mathbf{u}.$$

The velocity and pressure derivatives at the centroids are then given by

$$\mathbf{u}_c = \mathbf{R}_0\hat{\mathbf{u}},$$
$$\mathbf{p}_V = (\mathbf{L}_{22}^{\mathrm{T}})^{-1}[\mathbf{f}_c - \mathbf{M}_{22}\mathbf{R}_0\hat{\mathbf{u}} - (\mathbf{K}_{21} + \mathbf{K}_{22}\mathbf{R}_0)\hat{\mathbf{u}}]. \tag{28}$$

In this way the number of unknowns per element is reduced to 13. The pressure derivatives and velocities at the centroid can be derived by simple matrix–vector multiplications (equation (28)).

REFERENCES

1. M. Crouzeix and P. Raviart, 'Conforming and nonconforming finite element methods for solving the stationary Stokes equations I', *Rev. Franc. Automat. Informat. Rech. Oper.*, Ser rouge 7, no. R-3, 33–76 (1973).
2. D.F. Griffiths, 'Finite elements for incompressible flow', *Math. Meth. Appl. Sci.*, **1**, 16–31 (1979).
3. A. Segal, 'A review of some finite element methods to solve the stationary Navier–Stokes equations', *Int. j. numer. methods fluids*, **5**, 269–280 (1985).
4. R. L. Sani, B. E. Eaton, P. M. Gresho, R. L. Lee and S. T. Chan, 'On the solution of the time-dependent incompressible Navier–Stokes equations via a penalty Galerkin finite element method', *Proc. Second Int. Conf. Num. Meth. Lam. Turb. Flow.*, Venice, 1981, pp. 41–51.
5. P. M. Gresho, R. L. Lee and R. L. Sani, 'On the time-dependent solution of the incompressible Navier–Stokes equations in two and three dimensions', C. Taylor and K. Morgan (eds), in *Recent advances in numerical methods in fluids*, vol. 1, Pineridge press Ltd, Swansea U.K., 1980, pp. 27–80.
6. D. J. Tritton, 'Experiments on the flow past a circular cylinder at low Reynolds numbers', *J. Fluid Mech.*, **6**, 547–567 (1959).
7. G. K. Batchelor, '*An Introduction to Fluid Dynamics*, Cambridge University Press, 1979
8. F. Thomasset, '*Implementation of Finite Element Methods for Navier–Stokes equations*', Springer-Verlag, New York, 1981.
9. R. L. Sani, P. M. Gresho, R. L. Lee, D. F. Griffiths and M. Engelman, 'The cause and cure(?) of the spurious pressure generated by certain FEM solutions of the incompressible Navier–Stokes equations, Parts 1 and 2', *Int. j. numer. methods fluids.*, **1**, 17–43 and 171–204 (1981).
10. J. N. Reddy, 'On penalty function methods in finite element analysis of flow problems', *Int. j. numer. methods fluids.*, **2**, 151–171 (1982).
11. J. H. Schlichting, '*Boundary-Layer Theory*', 7th edn., McGraw-Hill, 1979.